First-Principles Modeling of A Miniature Tilt-Rotor Convertiplane in Low-Speed Operation

Guowei Cai,* Adnan Saeed, Fatima AlKhoori,† Ahmad Bani Younes, Tarek Taha, Jorge Dias, and Lakmal Seneviratne
Khalifa University, Abu Dhabi, UAE

ABSTRACT

In this paper, we present a comprehensive first-principles model that is developed for a miniature tilt-rotor convertiplane with Y-6 configuration. First, a flight dynamics model architecture is proposed based on the physical principle of the tilt-rotor convertiplane. Next, the parameter identification is conducted to determine the numerical values of all necessary parameters. The model fidelity is finally evaluated using practical data collected in flight experiments

1 INTRODUCTION

Miniature Unmanned Aerial Vehicles (UAVs) have recently gained significant popularities in both defence and civil applications. In general, miniature UAVs are dominated by two types: fixed-wing and rotorcraft, and each of which, however, has inherent limitations. A fixed-wing UAV generally advances in payload capacity, flight range, and endurance but requires runways or special equipments for take-off and landing. On the other hand, a rotorcraft UAV features the unique hovering capability and versatility but its speed and endurance limit significantly trunks its applications in missions requiring wide coverage or long endurance. As such, a new trend of miniature UAV design, which integrates the advantages of both and contributes to a much broader range of applications, has been recently explored. As a result, the Hybrid UAV, or fixed-wing Vertical Take-Off and Landing (VTOL) UAV, is born.

The miniature hybrid UAVs available in the market are categorized into two types: convertiplane UAVs and tail-sitter UAVs. A convertiplane maintains its airframe orientation in all flight modes, and certain transition mechanisms such as tilting rotors or wings are required to achieve mode traverse. On the other hand, a tail-sitter is an aircraft that takes off and lands vertically on its tail, and the the entire airframe needs to tilt to accomplish cruise flight. Recently, the convertiplane shows a much enhanced popularity over the tail-sitter, which is partially due to the non-airframe-transition, equivalent maneuverability, more robustness to environmental disturbances, and sufficient payload. Inspired by its popularity, we select a miniature tilt-rotor convertiplane with Y-6 rotor configuration (i.e., tri-copter with coaxial motor setup), named FireFLY6 and illustrated in Fig. 1, is selected as our research platform.

Figure 1: FireFLY6 miniature convertiplane.

In the procedure of a UAV development, establishing a reliable model that is able to capture the flight dynamics accurately over the flight envelope of interest is critically important. For the case of hybrid UAV, the modeling work is much more challenging, given its complicated mechanical design and aerodynamic features. A number of modeling work (see, e.g., [1] [2] [3] [4]) have been documented in the literature. Our survey provides two observations: 1) no systematic modeling work for the hover or low-speed operation, which is an essential flight condition but challenging to be modeled, and 2) very rare work provide model fidelity validation based on flight-test data. Inspired by such niche, in this paper we intend to present a first-principles modeling work for our tilt-rotor convertiplane at low-speed range, and further prove the model fidelity via a comparison between the actual flight data and simulation model responses.

The remaining content of this paper is organized as follows: In Section 2, a complete first-principles modeling architecture is proposed. Section 3 presents the procedure on determining the physical parameters involved in the proposed model. In Section 4, the fidelity of the model is comprehensively examined. Finally, Section 5 draw some key conclusions.

2 FIRST-PRINCIPLES FLIGHT DYNAMICS MODEL

In this section, a flight dynamics model architecture is proposed. The flight dynamics of a tilt-rotor convertiplane

*Corresponding author
†Research and Development Engineer at Emirates Technology and Innovation Center (ETIC), Abu Dhabi, UAE

http://www.imavs.org/

http://www.imavs.org/

over the low-speed envelope consists of five key elements: 1) kinematics, 2) six degree-of-freedom (6-DOF) rigid-body dynamics, 3) forces and moments generated by the rotors, 4) aerodynamic forces and moments of the fuselage, and 5) on-board stabilizer dynamics. To simplify the model, it is assumed that the aircraft operates in a rather calm environment. Consequently, wind effect can be omitted.

2.1 Kinematics

The kinematics component addresses the relative translation and rotation between a multi-rotor vehicle and the local environment. Two coordinate systems are involved: the body frame and the local North-East-Down (NED) coordinate frame. The kinematics can then be expressed by

$$\begin{cases} \dot{\mathbf{P}}_{\mathrm{n}} &= \mathbf{R}_{\mathrm{n/b}}\,\mathbf{V}_{\mathrm{b}} \\ \dot{\mathbf{\Phi}} &= \mathbf{S}_{\mathrm{n/b}}\,\boldsymbol{\omega}_{\mathrm{b}} \end{cases} \tag{1}$$

where $\mathbf{P}_{\mathrm{n}} = [\,p_{\mathrm{x}} \quad p_{\mathrm{y}} \quad p_{\mathrm{z}}\,]'$ is the position vector expressed in the local NED frame, $\mathbf{\Phi} = [\,\phi \quad \theta \quad \psi\,]'$ is the Euler angle vector, $\mathbf{V}_{\mathrm{b}} = [\,u \quad v \quad w\,]'$ and $\boldsymbol{\omega}_{\mathrm{b}} = [\,p \quad q \quad r\,]'$ are the body-axis velocities and angular rates. $\mathbf{R}_{\mathrm{n/b}}$ and $\mathbf{S}_{\mathrm{n/b}}$ are the corresponding rotation matrices and their expressions can be found in many textbooks such as [5].

2.2 6DOF Rigid-Body Dynamics

The 6-DOF rigid-body equation of motion representing a vehicle's translational and rotational movements in its body frame are defined by

$$\begin{cases} \dot{\mathbf{V}}_{\mathrm{b}} &= -\boldsymbol{\omega}_{\mathrm{b}} \times \mathbf{V}_{\mathrm{b}} + \dfrac{\mathbf{F}_{\mathrm{b}}}{m} + \dfrac{\mathbf{F}_{\mathrm{g}}}{m} \\ \dot{\boldsymbol{\omega}}_{\mathrm{b}} &= \mathbf{J}^{-1}\left[\mathbf{M}_{\mathrm{b}} - \boldsymbol{\omega}_{\mathrm{b}} \times (\mathbf{J}\,\boldsymbol{\omega}_{\mathrm{b}})\right] \end{cases} \tag{2}$$

where m is the vehicle's mass, $\mathbf{J} = diag\{J_{\mathrm{xx}}, J_{\mathrm{yy}}, J_{\mathrm{zz}}\}$ is the moment of inertia matrix, $\mathbf{F}_{\mathrm{g}}$ is the gravity force projected onto the body frame, and $\mathbf{F}_{\mathrm{b}}$ and $\mathbf{M}_{\mathrm{b}}$ are the aerodynamic forces and moments. Their expressions are particularly essential to fidelity of the derived first-principles modeling. For the case of the tilt-rotor convertiplane, they are mainly generated by the multiple rotors $\mathbf{F}_{\mathrm{rt}}$ and the fuselage $\mathbf{F}_{\mathrm{f}}$. Their detailed expression will be addressed below.

$$\begin{cases} \mathbf{F}_{\mathrm{b}} &= \mathbf{F}_{\mathrm{rt}} + \mathbf{F}_{\mathrm{f}} \\ \mathbf{M}_{\mathrm{b}} &= \mathbf{M}_{\mathrm{rt}} + \mathbf{M}_{\mathrm{f}} \end{cases} \tag{3}$$

2.3 Forces and Moments Generated by Rotors

Forces and moments determination related to multiple rotors is important in establishing the dynamics model. Particularly, for the convertiplane with Y-6 rotor configuration, the performance interference between the upper and lower rotors needs to be considered carefully. Before going to the detailed analysis, three reasonable assumptions are made as follows:

1. The coaxial rotors require the same rotation speeds for torque balance.
2. The performance of the upper rotor is not influenced by the lower rotor.
3. Only half of the area of the lower rotor operates in an effective climb velocity induced by the upper rotor.

Combining the analysis based on the Momentum Theory [6] and force/torque expression introduced in [7], we obtain

$$\begin{cases} T_{j,U} &= C_{\mathrm{T,j}}\,\rho\,\Omega_{j,U}^2\,d_{\mathrm{rt}}^4 \\ Q_{j,U} &= C_{\mathrm{P,j}}\,\rho\,\Omega_{j,U}^2\,d_{\mathrm{rt}}^5/(2\pi) \\ \Omega_{j,U} &= K_{\mathrm{rt}}\,r_{j,U} + \Omega_{\mathrm{hov}} \end{cases} \tag{4}$$

$$\begin{cases} T_{j,D} &= k_{\mathrm{intf}} C_{\mathrm{T,j}}\,\rho\,\Omega_{j,D}^2\,d_{\mathrm{rt}}^4 \\ Q_{j,D} &= C_{\mathrm{P,j}}\,\rho\,\Omega_{j,D}^2\,d_{\mathrm{rt}}^5/(2\pi) \\ \Omega_{j,D} &= K_{\mathrm{rt}}\,r_{j,D} + \Omega_{\mathrm{hov}} \end{cases} \tag{5}$$

where the subscript U(D) denotes the upper(lower) rotor belong to the same coaxial rotor set, the subscript j stands for j^{th} rotor set marked in the previous figure, C_{T} and C_{P} are dimensionless thrust and power coefficients, ρ is the air density, Ω is the motor rotation speed, d_{rt} is the rotor diameter, r is the normalized PWM-based motor driving input with the range of [-1, 1], k_{intf} is the thrust factor from interference, K_{rt} is the scaling factor of rotation speed change to normalized joystick input deflection, and Ω_{hov} is the rotation speed at hover. Note that

1. C_{T} and C_{P} can be determined either via ground experiments or based on the wind-tunnel test data which is available online (see, for example, [8]).
2. Due to the motor's extremely fast response, a simple proportional relationship (using hover condition as the trim) is utilized in the first-principles model.
3. The constant value of k_{intf} is based on the Momentum Theory, given the case of balanced torques [6].
4. Given the assumption 1 and the Y-6 configuration, all the six rotors share an identical RPM, that is, Ω_{hov}, at ideal hover.

Both the translational and rotational movements of the vehicle leads to slight flapping motion of the rotor blade. To account for this effect, a quasi-steady rotor flapping expression, proposed in [9], is adopted in our modeling process, and defined by:

$$\begin{cases} \beta_{\mathrm{lc},j} &= (K_{\mathrm{ab1}}q + K_{\mathrm{ab2}}p - K_{\mathrm{ab3}}u - K_{\mathrm{ab4}}v)/K_{\mathrm{ab5}} \\ \beta_{\mathrm{ls},j} &= (-K_{\mathrm{ab1}}p + K_{\mathrm{ab2}}q - K_{\mathrm{ab3}}v + K_{\mathrm{ab4}}u)/K_{\mathrm{ab5}} \end{cases} \tag{6}$$

where $\beta_{\mathrm{lc},j}$, and $\beta_{\mathrm{ls},j}$ are the longitudinal and lateral flapping angles, K_{ab1} to K_{ab5} are the lumped derivatives whose detailed definitions can be found in [9]. Is should be highly noted that due to the above definition, the upper and lower

http://www.imavs.org/

rotors of the same coaxial rotor set share the same flapping angles. Therefore, no subscript U and D are used in the above equation. With the flapping angles defined, the force and moment vectors of the upper and low rotors are calculated by:

$$\begin{cases} \mathbf{F}_{\mathrm{rt},j,U} &= [\,T_{j,U}\,\mathbf{s}(\beta_{\mathrm{lc}}) \quad -T_{j,U}\,\mathbf{s}(\beta_{\mathrm{ls}}) \quad -T_{j,U}\,\mathbf{c}(\beta_{\mathrm{lc}})\,\mathbf{c}(\beta_{\mathrm{ls}})\,]' \\ \mathbf{F}_{\mathrm{rt},j,D} &= [\,T_{j,D}\,\mathbf{s}(\beta_{\mathrm{lc}}) \quad -T_{j,D}\,\mathbf{s}(\beta_{\mathrm{ls}}) \quad -T_{j,D}\,\mathbf{c}(\beta_{\mathrm{lc}})\,\mathbf{c}(\beta_{\mathrm{ls}})\,]' \end{cases} \tag{7}$$

$$\begin{cases} \mathbf{M}_{\mathrm{rt},j,U} &= [\,0 \quad 0 \quad \pm Q_{j,U}\,]' \\ \mathbf{M}_{\mathrm{rt},j,D} &= [\,0 \quad 0 \quad \pm Q_{j,D}\,]' \quad (+\text{ for CW}) \end{cases} \tag{8}$$

The aerodynamic drag caused by the fuselage of multi-rotor vehicles is generally small and can thus be ignored. Therefore, the combined aerodynamic force $\mathbf{F}_{\mathrm{b}}$ and moment $\mathbf{M}_{\mathrm{b}}$ can be reduced to:

$$\begin{cases} \mathbf{F}_{\mathrm{rt}} &= \sum_{j=1}^{n} (\mathbf{F}_{\mathrm{rt},j,U} + \mathbf{F}_{\mathrm{rt},j,D}) \\ \mathbf{M}_{\mathrm{rt}} &= \sum_{j=1}^{n} (-\mathbf{M}_{\mathrm{rt},j,U} - \mathbf{M}_{\mathrm{rt},j,D} + l_{j,U} \times \mathbf{F}_{\mathrm{rt},j,U} + l_{j,D} \times \mathbf{F}_{\mathrm{rt},j,D}) \end{cases} \tag{9}$$

where $l_{j,U/D}$ is the body-frame position vector of the jth upper (lower) rotor with respect to the center of gravity (CG).

2.4 Forces and Moments of Fuselage

A unique feature of the low-speed operation of a tilt-rotor convertiplane is the aerodynamic forces and moments generated by its fuselage. From the perspective of aerodynamic effect, there are generally three force components: lift, drag, and side forces. Each of the three force components is further associated with a moment generation. Furthermore, in low-speed operation, the side force and moments are sufficiently small and thus can be omitted.

As for the lift and drag analysis, stripe theory is adopted in our work to achieve sufficient accuracy. More specifically, the entire fuselage was divided into multiple sections along the starboard with sufficiently small span value. For each section, we have

$$\begin{cases} \Delta L &= \frac{1}{2}\rho \Delta A V_{\mathrm{local}}^2 C_{\mathrm{l,b}} \\ \Delta D &= \frac{1}{2}\rho \Delta A V_{\mathrm{local}}^2 C_{\mathrm{d,b}} \end{cases} \tag{10}$$

where ΔL and ΔD are the sectional lift and drag forces, ΔA is the effective fuselage area for lift and drag generation, V_{local} is the local total velocity at the current section, $C_{\mathrm{l,b}}$ and $C_{\mathrm{d,b}}$ are the lift and drag coefficients for the current section

Once the sectional lift and drag forces are determined, the decomposition to the body frame needs to be conducted as follows

$$\begin{cases} \Delta F_{\mathrm{f,x}} &= -L\,\mathbf{s}(\alpha_{\mathrm{in}}) - D\,\mathbf{c}(\alpha_{\mathrm{in}}) \\ \Delta F_{\mathrm{f,z}} &= -L\,\mathbf{c}(\alpha_{\mathrm{in}}) + D\,\mathbf{s}(\alpha_{\mathrm{in}}) \end{cases} \tag{11}$$

where α_{in} is the incidence angle.

The corresponding moment is calculated by

$$\Delta M_{\mathrm{f}} = \Delta F_{\mathrm{f}} \times l_{\mathrm{ae}} \tag{12}$$

where $l_{\mathrm{ae}} = [\,x_{\mathrm{ae}} \quad y_{\mathrm{ae}} \quad z_{\mathrm{ae}}\,]'$ is the aerodynamic center's location with respect to the CG.

The overall aerodynamic force and moment generated by the fuselage is achieved by integrating the sectional forces and moments along the starboard.

2.5 On-board Stabilizer Dynamics

The last dynamics component of the first-principles modeling is related to the on-board stabilizer module, which is widely used in multi-rotor vehicles to dampen the rotor response. In our work, we employ an open-source stabilizer module, named Pixhawk, with configurable PID control structure and control gains. Its stabilization mechanism is shown in Fig. 2. More specifically,

1. For the rolling and pitching dynamics, both Euler angle (ϕ or θ) and angular rate (p or q) are fed back to the stabilizer. Two successive control loops are included: PID control structure is adopted in the inner loop for angular rate stabilization, whereas P control is adopted in the outer loop for Euler angle stabilization.

2. For the heave dynamics, vertical acceleration (a_{z}) is fed back for stabilization, which is achieved by a single PI control loop.

3. For the yawing dynamics, both heading angle Ψ and yaw rate r are fed back to the stabilizer. Two successive control loops are adopted: PI control structure is adopted in the inner loop for yaw rate stabilization, whereas P control is adopted in the outer loop for heading angle stabilization.

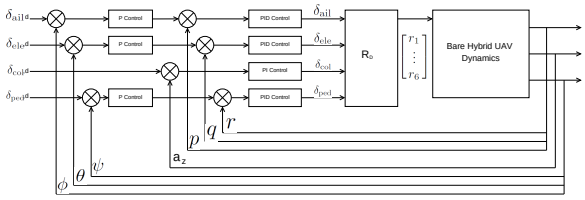

Figure 2: Onboard stabilizer dynamics.

Finally, the stabilizer module also acts as a signal distributor, converting the driving commands to motor-recognized control signals for n motors (i.e., r_1 to r_6), realized by

$$\begin{bmatrix} r_1 \\ \vdots \\ r_6 \end{bmatrix} = R_{\mathrm{D}} \begin{bmatrix} \delta_{\mathrm{ail}} \\ \delta_{\mathrm{ele}} \\ \delta_{\mathrm{col}} \\ \delta_{\mathrm{ped}} \end{bmatrix} \tag{13}$$

where R_{D} is 6×4 signal distribution matrix given by

$$R_{\mathrm{D}} = \begin{bmatrix} 1 & 1 & 1 & 1 \\ 1 & 1 & 1 & -1 \\ -1 & 1 & 1 & 1 \\ -1 & 1 & 1 & -1 \\ 0 & -1 & 1 & 1 \\ 0 & -1 & 1 & -1 \end{bmatrix} \tag{14}$$

3 PARAMETER IDENTIFICATION

To complete the first-principles modeling, a set of physical parameters are required to be determined. These parameters are categorized into three types, including: 1) parameters that can be measured directly, 2) parameters that can be determined via computer-aided-design (CAD), and 3) parameters that need to be determined experimentally. Note that

1. In Table 1, all the parameters that can be measured directly are summarized in the first category.

2. CAD software such as SolidWorks can be adopted as an efficient tool to determine the physical properties of the fuselage and rotor blades. The virtual hybrid UAV built in the CAD environment is required to maximally match the actual one, in terms of physical dimension and material property. Fig. 3 illustrate the virtual and real FireFLY6 platforms, and the related parameters are summarized in the second category of Table 1.

Figure 3: Virtual and actual FireFLY6 hybrid UAVs.

3. The aerodynamic coefficients for the propellers are determined either via wind-tunnel or ground experiment, depending on the availability of the wind-tunnel test data. Recently, thorough research and wind-tunnel experiments have been carried out for hobby-based propellers and representative airfoils, and the associated results are accessible in the literature or online databases (see, e.g., [8]). However, if such data is not available, particularly to certain newly developed propellers, dynamometer-based experiment should be conducted, in which the thrust and torque values at different rotation speeds should be recorded for determining the coefficients via data curve-fitting.

4. The lift, drag, and moment coefficients for the sectional fuselage can be either determined via wind-tunnel or using simulation toolkit. The latter is preferable in our work given its availability and efficiency. A popular software analysis toolkit named XFLR5 is adopted to generate these coefficients over the complete range of angle of attack [-π, π], assuming a uniform airfoil is applied to the entire flying-wing fuselage. The resulting coefficients are obtained in the lookup table format, and plotted in Figs. 4 to 6 for convenient reference.

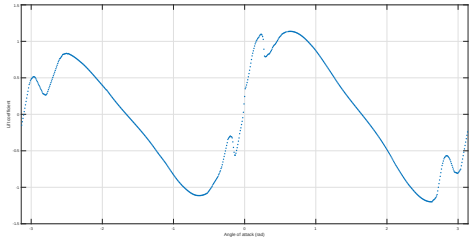

Figure 4: Lift coefficient of the selected airfoil at ultra-low Reynolds number.

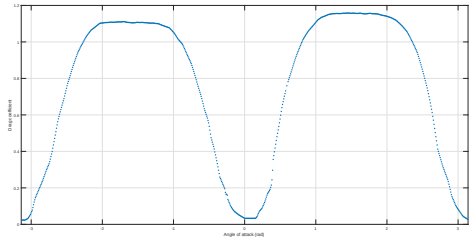

Figure 5: Drag coefficient of the selected airfoil at ultra-low Reynolds number.

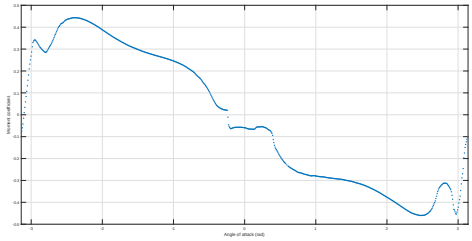

Figure 6: Moment coefficient of the selected airfoil at ultra-low Reynolds number.

5. As for the on-board stabilizer, if the control structure and control gains are configurable, their values can be

http://www.imavs.org/

http://www.imavs.org/

obtained directly. For the case of FireFLY6, these parameters are summarized in the third category of Table 1. If these information are not available, two types of ground experiments are required to initially estimate the parameters related to the on-board stabilizer. The former is for determining the scaling factors, in which the hybrid UAV is required to be fixed onto a testing-rig with only one free degree of freedom (i.e., roll, pitch, heave, or yaw), and step input is injected into one of the four input channels. Both the input and the corresponding output should be recorded for scaling factor determination. The second experiment is conducted for estimating the PI/PID control gains and the signal distribution matrix. The control gains and distribution matrix can be determined via input-output data curve-fitting.

Table 1: Parameters required for FireFLY6 first-principles modeling.

Category	Symbol	Value	Unit
1	c	0.027	m
1	d_{rt}	0.255	m
1	m	2.71	kg
1	ρ	1.16	kg m^{-3}
2	J_{xx}	0.0945	kg m^2
2	J_{yy}	0.0816	kg m^2
2	J_{zz}	0.1691	kg m^2
2	I_β	3.72 e-9	kg m^2
2	k_β	0.251	N m rad^{-1}
3	K_ϕ	5	NA
3	$K_{P,p}$	0.12	NA
3	$K_{I,p}$	0.002	NA
3	$K_{D,p}$	0.003	NA
3	K_θ	5.5	NA
3	$K_{P,q}$	0.12	NA
3	$K_{I,q}$	0.002	NA
3	$K_{D,q}$	0.003	NA
3	K_ψ	2.8	NA
3	$K_{P,r}$	0.22	NA
3	$K_{I,r}$	0.02	NA
3	$K_{D,r}$	0.002	NA
3	$K_{P,az}$	2	NA
3	$K_{I,az}$	0.0015	NA

4 MODEL VALIDATION

Model validation has been be conducted based on multiple flight experimental data. Frequency sweep, which refers to a class of control inputs that has a quasi-sinusoidal shape of increasing frequency [10], is adopted as the input signal because it is relatively easy to issue and can persistently perturb the frequency band of interest. Each individual perturbation starts with the hovering condition. The frequency sweep, which is issued by an human pilot, is then sequentially injected into one of the four input channels to excite the flight dynamics. Meanwhile, the pilot maintains the rough trim condition by issuing minimum and uncorrelated control signals in the remaining input channels. The same procedure is repeated for the remaining joystick inputs. As a result, four types of perturbations are recorded.

The validation results are depicted in Figs. 7 to 12, which all belong to the elevator channel perturbation. Note that for each output response, a fairly good matching has been achieved. Mismatch can be still observed, which is mainly caused by the omittance of certain flight dynamics mode, the simplified model architecture of several flight dynamics modes included, and the environmental disturbances that are not modeled in the current work.

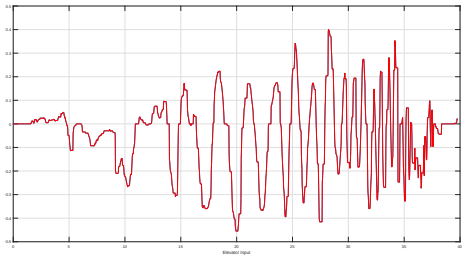

Figure 7: Elevator input.

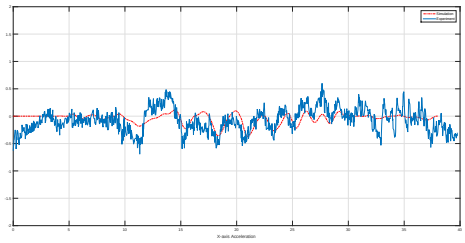

Figure 8: X-axis acceleration.

5 CONCLUSION

In this paper, we have proposed a feasible first-principles model for a Y-6 hybrid UAV. Parameter identification is discussed and flight test data collected in the low-speed range are adopted for model fidelity validation. The future work will concentrate on the following key issues: 1) enhanced first-principles architecture, 2) enhanced parameter identification procedure with higher accuracy, 3) more comprehensive evaluation with necessary analysis, and 4) an in-depth analysis on

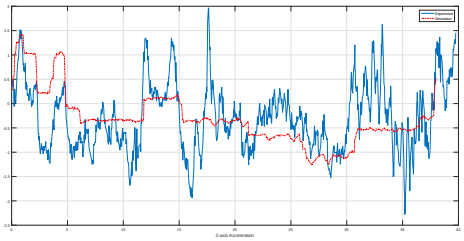

Figure 9: Z-axis acceleration.

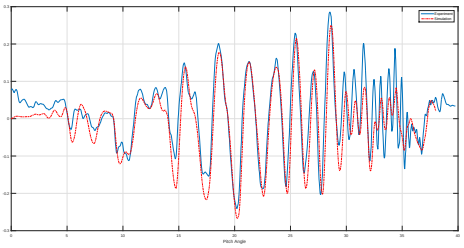

Figure 11: Pitch angle.

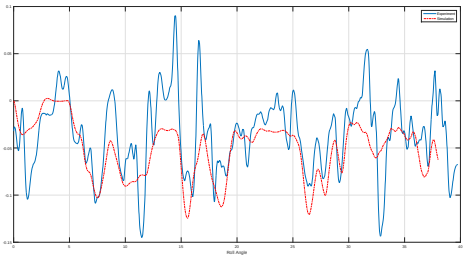

Figure 10: Roll angle.

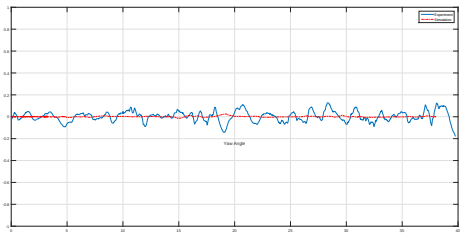

Figure 12: Heading angle.

the necessity and contribution of the dynamic components involved in structuring the first-principles model.

REFERENCES

[1] Kaan Taha Öner, Ertuğrul Çetinsoy, Mustafa Ünel, Mahmut Faruk Akşit, Ilyas Kandemir, and Kayhan Gülez. Dynamic model and control of a new quadrotor unmanned aerial vehicle with tilt-wing mechanism. 2008.

[2] Kaan Taha Öner, Ertuğrul Çetinsoy, EFE SIRIMOĞLU, Cevdet Hançer, Mustafa Ünel, Mahmut Faruk Akşit, Kayhan Gülez, and Ilyas Kandemir. Mathematical modeling and vertical flight control of a tilt-wing uav. *Turkish Journal of Electrical Engineering & Computer Sciences*, 20(1):149–157, 2012.

[3] Pierre-Richard Bilodeau and Franklin Wong. Modeling and control of a hovering mini tail-sitter. *International Journal of Micro Air Vehicles*, 2(4):211–220, 2010.

[4] J Escareno, S Salazar, and R Lozano. Modeling and control of a convertible vtol aircraft. In *45th IEEE Conference on Decision and Control, San Diego, California*, pages 13–15. Citeseer, 2006.

[5] Guowei Cai, Ben M Chen, and Tong Heng Lee. *Unmanned rotorcraft systems*. Springer Science & Business Media, 2011.

[6] J Gordon Leishman. *Principles of Helicopter Aerodynamics with CD Extra*. Cambridge university press, 2006.

[7] John B Brandt and Michael S Selig. Propeller performance data at low reynolds numbers. In *49th AIAA Aerospace Sciences Meeting*, pages 2011–1255, 2011.

[8] Gavin Ananda et al. Uiuc propeller database. *URL: http://www. ae. illinois. edu/m-selig/props/data/apce_9x4. 5_jb1000_6917. txt,[cited 15 Feb 2011]*, 2008.

[9] Pierre-Jean Bristeau, Philippe Martin, Erwan Salaün, Nicolas Petit, et al. The role of propeller aerodynamics in the model of a quadrotor uav. In *European control conference*, volume 2009, 2009.

[10] Mark B Tischler and Robert K Remple. *Aircraft and rotorcraft system identification: engineering methods with flight test examples*. Reston: American Institute of Aeronautics and Astronautics, 2006.

http://www.imavs.org/